ELSEVIER

Journal of Power Sources 106 (2002) 178–188

JOURNAL OF POWER SOURCES

www.elsevier.com/locate/jpowsour

Ni–YSZ cermet anodes prepared by citrate/nitrate combustion synthesis

Marjan Marinšek*, Klementina Zupan, Jadran Maèek

Faculty of Chemistry and Chemical Technology, University of Ljubljana, Aškerèeva 5, 1000 Ljubljana, Slovenia

Abstract

The synthesis of Ni–YSZ cermets with tailored particle package, shape and microstructural characteristics is essential when preparing anodes for solid oxide fuel cells (SOFC). These materials are generally prepared by sintering and subsequent reduction of the mixture of metal oxides. In order to obtain cermets with an adequate contact area between electrocatalyst (Ni) and ionic conductor (YSZ), an alternative route was used based on mixed gel combustion with the material synthesis, calcination and partial sintering achieved in one step. The precursor for the combustion synthesis was a mixed citrate/nitrate gel prepared from nickel, zirconium and yttrium nitrates and citric acid by vacuum evaporation of the solution. The combustion reaction of this gel produces submicrometer crystalline NiO–YSZ composite. The influence of the fuel/oxidant molar ratio of the precursor on the combustion rate and end product characteristics was investigated. The reaction period, phase composition, morphology and agglomerate formation were studied in detail. It was shown that the initial fuel/oxidant ratio strongly influences the characteristics of the powder mixtures thus obtained. The morphological properties of the prepared mixed oxides after the combustion synthesis reveal that the particle size distribution and the agglomerate formation in the voluminous intermediate mixed oxide product (green body) differ with the initial fuel/oxidant molar ratio. Narrower agglomerate and pore size distribution has a great influence on the subsequent sintering and reduction of the mixed material. If the particle and pore size distribution in the green body are narrow, the coarsening of the YSZ and NiO grains, and subsequently, YSZ and Ni grains are less pronounced.

Keywords: Ni–YSZ cermet anodes; Solid oxide fuel cells; Citrate/nitrate combustion synthesis

1. Introduction

Due to their high efficiency and environmentally friendly nature, solid oxide fuel cells (SOFC) are considered to be one of the most promising energy converters in the future [1,2]. The most frequently used SOFC system consists of yttria-stabilized zirconia (YSZ) as an electrolyte, the cermet of nickel and YSZ (Ni–YSZ) as an anode, the electrically conducting oxides based on lanthanum manganites $La_{1-x}M_xMnO_3$ (M = Sr, Ba, Ca) as cathode, and doped lanthanum chromate $La_{1-y}M_yCrO_3$ (M = Sr, Ca, Mg) as an interconnect material [3–7]. The Ni–YSZ cermet is generally used as the anode in SOFC stack because of the reducing conditions in the SOFC anode department, low cost of Ni and its relatively high electrocatalytic activity in gas reforming and subsequent H_2 oxidation [8]. YSZ in cermet serves as a supporting framework for Ni particles, thus, ensuring anode thermal expansion acceptably close to other SOFC components [9]. The Ni–YSZ composite has to meet certain criteria in order to act as an effective anode material. It should have high electronic conductivity, appropriately porous microstructure (approximately 30% open porosity) and physical and chemical compatibility with other cell components [10]. Furthermore, both the Ni and YSZ phase should form continuous network structure respectively in order to extend the effective Ni–YSZ–fuel triple-phase boundary deep into the anode layer.

All these requirements, to a large degree, are controlled by the cermet microstructure. Numerous studies have shown the importance of the anode layer microstructure development, including initial anode material particle properties, e.g. particle size distribution, the degree of agglomeration, and metal to ceramic phase ratio [9,11–13]. The main problem in developing the anode layer comes from the extended Ni particle-coarsening during thermal treatment and subsequent cell operation [14]. Although the loss of the percolation between metallic grains with time and thus the decrease of the triple-phase boundary length cannot be avoided completely, it can be reduced substantially by choosing a preparation path which yields well-mixed (on nanoscale) narrow sized particles after the synthesis [15].

Among the various solution routes employed in the oxide materials preparation, the combustion synthesis seems to be very promising [16–18]. Starting with the solution of all

* Corresponding author.
E-mail address: marjan.marinsek@uni-lj.si (M. Marinšek).

0378-7753/02/$ – see front matter
PII: S0378-7753(01)01056-4

Table 1
Sample preparation conditions

Sample	$Citrate_{initial}$ (mmol)	$Nitrate_{initial}$ (mmol)	c/n[a]	Combustion velocity (g/s)	Color of an as-synthesized product
A	12.9	99.9	0.13	No self-sustaining reaction	Pale green
B	14.0	99.9	0.14	Reaction gel has to be ignited several times	Pale green
C	14.9	99.9	0.15	0.05	Green
D	17.9	99.9	0.18	0.09	Green
E	23.0	99.9	0.23	0.07	Black
F	28.0	99.9	0.28	0.03	Dark-gray
G	32.9	99.9	0.33	0.01	Dark-gray

[a] Citrate/nitrate initial molar ratio.

components, a maximum homogeneity of the mixed powder can be achieved. This method makes use of the strong exothermicity of redox reactions associated with the oxide synthesis. Such reactions proceed in the form of a self-sustaining front, which propagates through the reactants. Oxide powders are formed directly from the precursor gel.

Ni–YSZ cermet preparation by using combustion synthesis has already been successfully applied by some authors. Ringuede et al. [19] established the reaction system employing nitrates both as metal precursors and oxidizing reagents and urea as fuel component. Aruna et al. [20] prepared Ni–YSZ cermet powders using carbohydrazide as fuel component. Relatively high speed of propagated self-sustaining reaction front is achieved when combustion synthesis is based on nitrate–glycine [21] or Zr–NiO–Y_2O_3 [22] redox system.

The aim of this work was to apply the combustion synthesis technique based on the redox reaction system of metal nitrates and citric acid for the formation of Ni–YSZ composite. Different citrate/nitrate (c/n) initial molar ratios were used in order to manufacture ultrafine Ni–YSZ composite powders that are characterized by very uniform distribution of Ni particles. The microstructure and thermal characteristics of the composites thus prepared were studied to test the compatibility of the combustion-derived Ni–YSZ cermets in SOFC applications.

2. Experimental method

The Ni–YSZ composite powders (40 vol.% of Ni) were prepared by the modified combustion synthesis of citrate/nitrate gel. In this combustion method, the starting materials were $ZrO(NO_3)_2{\cdot}6H_2O$, Y_2O_3, $Ni(NO_3)_2{\cdot}6H_2O$ and citric acid (analytical reagent grade). $ZrO(NO_3)_2{\cdot}6H_2O$, $Ni(NO_3)_2{\cdot}6H_2O$ and citric acid were dissolved with minimum additions of water in the amounts which assure the desired final nickel content. Y_2O_3 was then added to the zirconyl nitrate aqueous solution in which a calculated amount of nitric acid (65%) was added. The Y_2O_3 addition was calculated to assure the final YSZ composition to be 90 mol.% of ZrO_2 and 10 mol.% of Y_2O_3. The three precursors were mixed together to prepare a solution with an appropriate citrate/nitrate molar ratio. The initial citrate/nitrate molar ratios in the reaction mixtures were altered from 0.13 to 0.33 as indicated in Table 1. A dish was kept over a water bath at 60 °C under vacuum (20 mmHg) until the solution transformed into a bright green gel. The gels were gently milled in an agate mortar and uniaxially pressed (17 MPa) into pellets (12 mm in diameter, height 30 mm). The samples were placed on an Al_2O_3 plate and ignited at the top of the pellets (Fig. 1). The reaction period was measured.

The amount of nickel in the samples was determined by a volumetric method. The samples were characterized by the X-ray powder diffraction technique using a Philips PW-1710 apparatus. Data were collected in the range from 15 to 75°, 2Θ, in steps of 0.04° for 1 s per step. TG analysis was performed on a Mettler TG-50 Thermobalance and DSC analysis on a Mettler standard cell DSC 20. A Micrometrics Gemini II 2370 was used to determine specific surface area of the samples by the BET method. After synthesis the samples were milled in the agate mortar for 5 min and unaxially pressed (170 MPa) into pellets, sintered at 1380 °C for 2 h in the air, while the reduction treatment was carried out at 950 °C under atmosphere of 4 vol.% of H_2 and 96 vol.% of Ar. The synthesized pellets and those obtained after the sintering and reduction were analyzed by optical microscopy (Leitz) and scanning electron microscope (SEM, Jeol T300). The shrinkage during sintering of all samples was measured by a Leitz–Wetzlar heating microscope. The ac impedance measurements of sintered samples were carried out using an impedance analyzer (Hewlett-Packard 4284A) over the frequency range from 20 Hz to 1 MHz.

3. Results and discussion

Combustion synthesis offers an alternative way for preparing mixed ultrafine metal oxides. The self-sustaining reaction was based on the combustion of citric acid with nitrates. According to the concepts employed in propellant

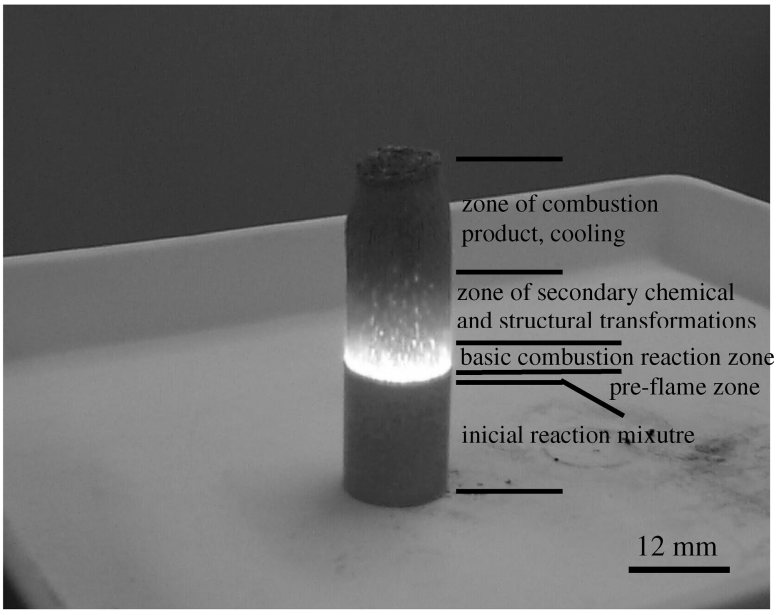

Fig. 1. Photograph of a typical citrate/nitrate gel combustion process of mixed oxide nanopowders.

chemistry, the three idealized reactions that proceed during the synthesis can be written as follows [23]:

$$9ZrO(NO_3)_2 + 5C_6H_8O_7 \rightarrow 30CO_2 + 9N_2 + 20H_2O + 9ZrO_2$$

$$18Y(NO_3)_3 + 15C_6H_8O_7 \rightarrow 90CO_2 + 27N_2 + 60H_2O + 9Y_2O_3$$

$$9Ni(NO_3)_2 + 5C_6H_8O_7 \rightarrow 30CO_2 + 9N_2 + 20H_2O + 9NiO$$

The burning mixture generates a large amount of heat and outcoming gases in a short period of time, thus, converting the precursor mixture to the product material. The vigorousness of the combustion process is strongly influenced by the initial c/n molar ratio. In our case, c/n initial ratio is a function of the fuel content in the precursor mixture since we altered the fuel addition. In general, the closer the initial c/n molar ratio to the stoichiometric value the more intensive the reaction (i.e. the consumption of the nitrates and fuel, and the formation of the target oxides). The calculated stoichiometric c/n initial molar ratio for the upper system is 0.28. However, the combustion velocity of the precursor gels was maximum when the initial c/n molar ratio was 0.18 and decreased both ways either with higher or lower initial c/n ratios (Table 1). The precursor mixture (4.70 g) with c/n initial molar ratio of 0.18 (Sample D) reacted over a period of 52 s, while the reaction mixtures with c/n initial ratios 0.33 (Sample G) and 0.15 (Sample C) took 367 and 96 s, respectively, for the same mass of the reacting gel. This phenomenon is probably due to the fact that, the precursor reaction mixture was kept over a water bath under vacuum for several hours. During that time a significant amount of initially present nitrates evaporate increasing the c/n ratio.

The vigorousness of the combustion process was followed by thermal analysis. We tried to simulate the combustion reaction of different reaction gels in DSC cell. Figs. 2 and 3 represent the curves of the combustion synthesis performed in argon and air, respectively. The results of DSC analysis indicate that the combustion synthesis proceeds over at least two separate steps. The first step at approximately 160 °C is strongly influenced by the fuel content in the reaction gel and the peak area increases with c/n initial ratio increase. According to some literature data [24,25], this step is attributed to the free citric acid decomposition and some nitric acid removal. Compared with the first step, the second step over a broad temperature range from 200 to 300 °C is more pronounced if the initial c/n ratio is small. The second DSC step is only slightly detectable if the initial c/n ratio is 0.33 (Sample G), while in the case of Sample A ($c/n = 0.13$) this step is represented by two successive peaks. Thermal behavior during the second DSC step is probably due to the decomposition of citrate complex and burning of citrate chains [25]. Both steps are very similar regardless of whether they were measured in argon (Fig. 2) or in air (Fig. 3) atmosphere. This indicates that they are both strongly connected with the combustion synthesis itself. DSC curves of different reaction gels measured in argon and air atmosphere differ significantly in the temperature range between 340 and 380 °C. During this third step the DSC response could be exothermic or endothermic depending on the atmosphere of the measurement. This step is probably not related to the combustion synthesis of the oxide powder but to the elimination of the residual citric acid. If the DSC measurement is taken in the air atmosphere, the residual citric acid burns yielding a strong exothermic effect (Fig. 3). Conversely, in argon atmosphere the residual citric acid is decomposed endothermically as indicated by DSC effect in Fig. 2.

As-synthesized samples were investigated by SEM analysis. Typical SEM photomicrographs of as-prepared ashes are shown in Figs. 4–6. Because of a large amount

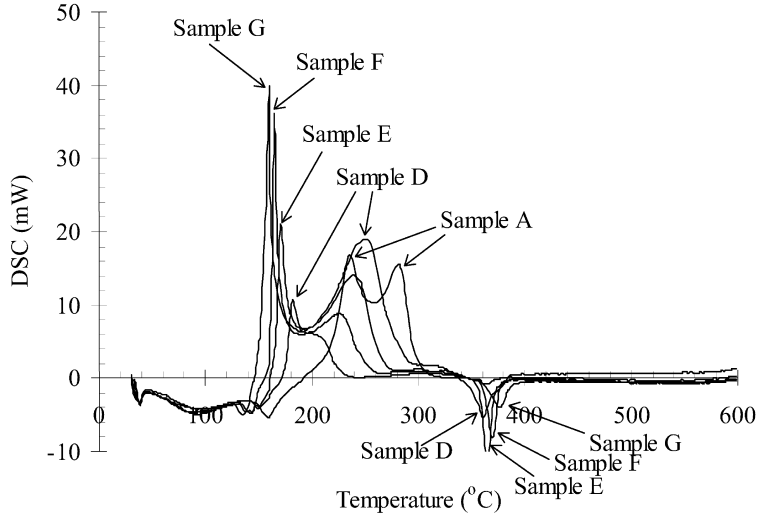

Fig. 2. DSC thermal analysis plots of different citrate/nitrate gel precursors taken in argon.

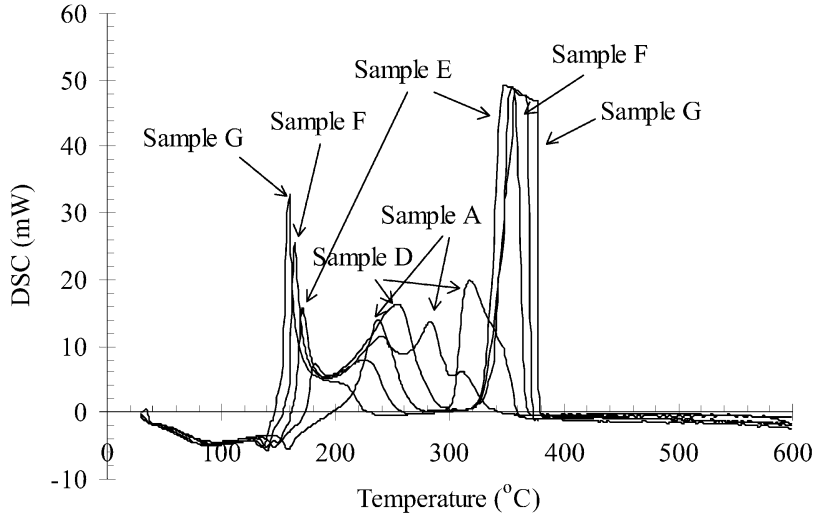

Fig. 3. DSC thermal analysis plots of different citrate/nitrate gel precursors taken in air.

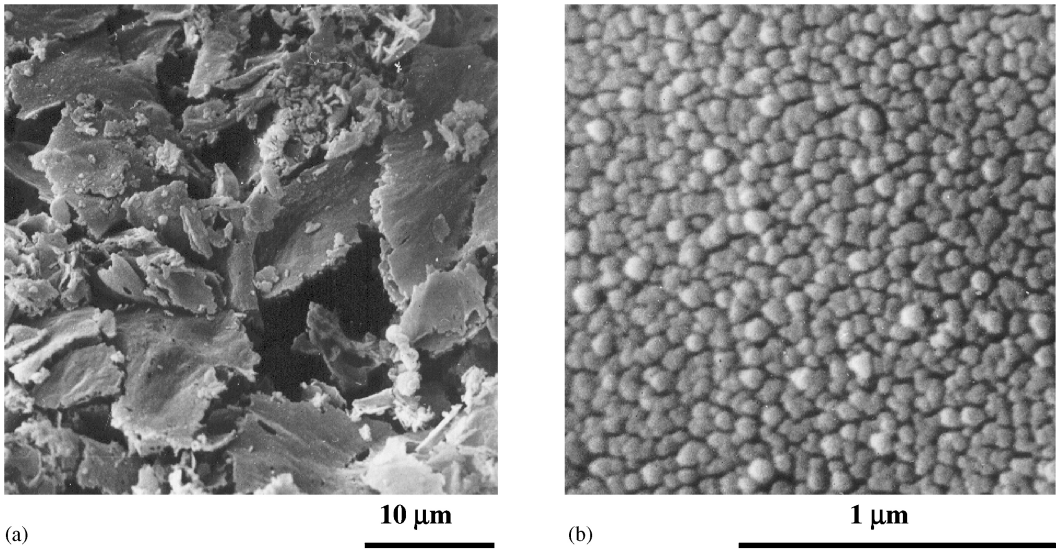

Fig. 4. SEM image (a and b) of a surface of as-prepared Sample A.

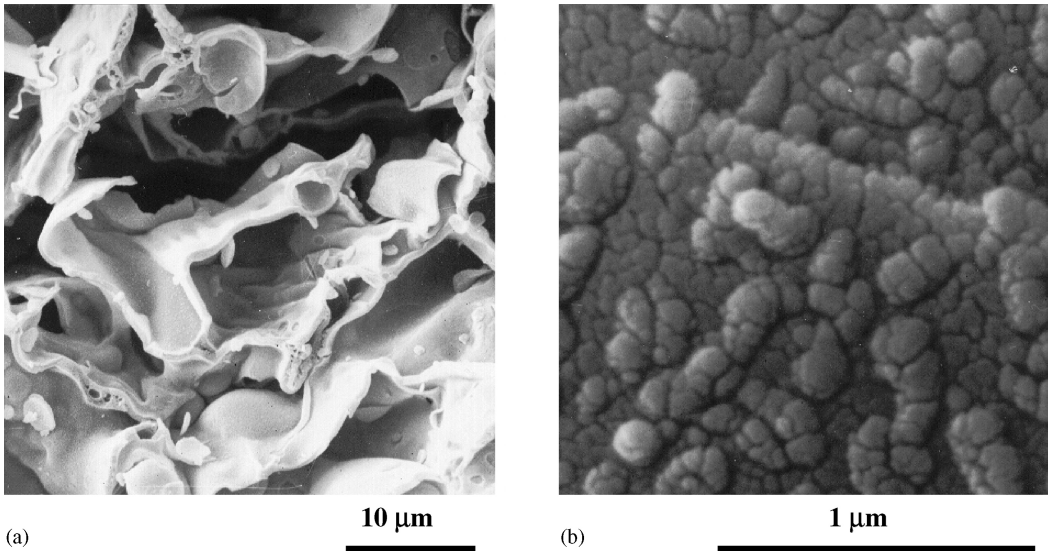

(a) (b)

Fig. 5. SEM image (a and b) of a surface of as-prepared Sample E.

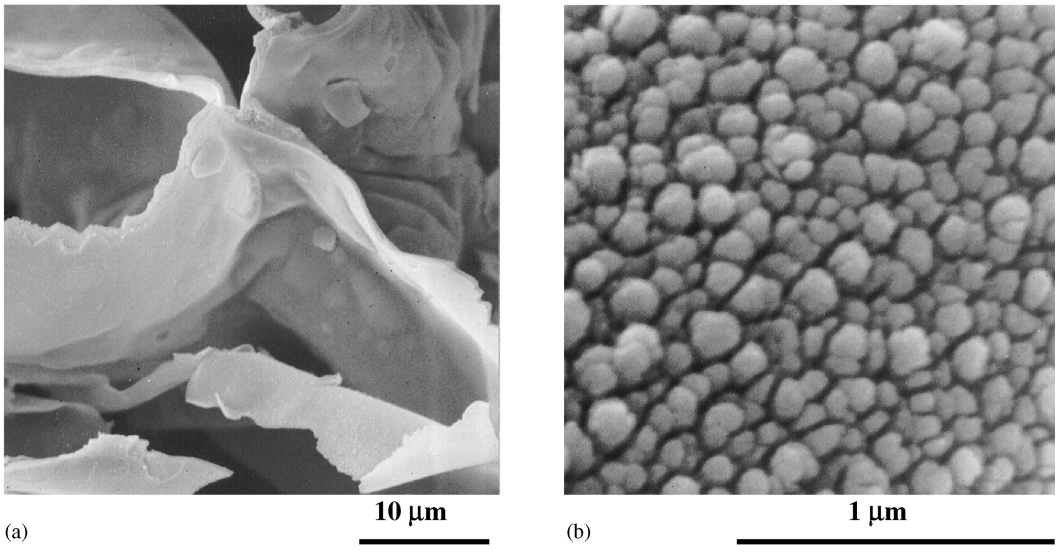

(a) (b)

Fig. 6. SEM image (a and b) of a surface of as-prepared Sample G.

of the outcoming gases as-prepared samples are rather voluminous and very fragile. The particles are bound together into agglomerates of different shapes and sizes. While the agglomerates of Samples E (Fig. 5a) and G (Fig. 6a) form a curtain-like shapes with broken hollow spheres, in Sample A (Fig. 4a) the agglomerates look like tinny lamellas. The nanosize nature of the combustion-derived powders was confirmed by SEM investigation at higher magnifications (Figs. 4b-6b). The agglomerates are composed of spherical particles packed close together. The average particle sizes of the non-agglomerated spherical particles are in the range of 50–80 nm (Sample A) and 80–150 nm (Samples E and G). The variances in the mean particle size between different, as-prepared powders are the consequence of the synthesis nature during the powder preparation. The particle size of the as-reacted material depends both on the conditions in the reaction zone where the combustion propagates and on the amount of disintegration that occurs during the combustion process. The reaction mixtures in which the c/n molar ratio prior to the ignition is close to the stoichiometric value (0.28), the reaction will proceed at higher propagation rates and higher temperatures compared to those with fuel or oxidant rich compositions. The higher reaction temperature may even cause sintering of the formed particles. Consequently, these particles will tend to grow as the reaction zone propagates through the pellet and leaves the reacted zone, which slowly cools down to a room temperature (Fig. 1). Cooling in a pellet is relatively slow because only a small portion of the reacted material is exposed to the outer atmosphere and the majority of the sample is captured in a hot core of the pellet. On the other hand, in the case of fuel or oxidant rich samples a portion of the starting materials (either metal nitrates or fuel)

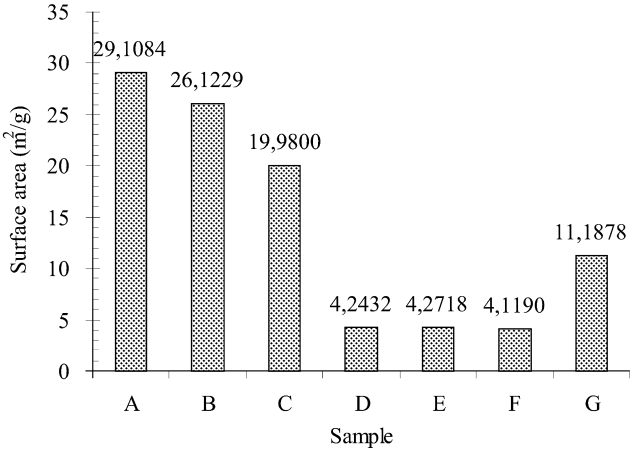

Fig. 7. Variation of the specific surface area in synthesized mixed powders using different initial c/n molar ratios.

does not participate in the mixed citrate/nitrate precursor formation. Especially, excess fuel may act as a space-filling template, which will leave empty spaces as the fuel burns during the reaction. Increasing the fuel content further would result also in more gas formation since there is more fuel to incinerate.

A strong influence of the fuel content used in the combustion reaction on the prepared powder was also observed both in SEM- and BET-specific surface area measurements (Fig. 7). The highest specific surface area was obtained for the powder prepared from the reaction mixture A (oxidant-rich sample). Afterwards, the specific surface area of the as-synthesized powders decreased as the initial c/n molar ration increased reaching its minimum in the case of Samples D, E and F (≈4.2 m^2/g). With even higher initial c/n ratio (Sample G), the specific surface area increased again as a consequence of the small size of the particles prepared in the latter case. Knowing the theoretical density and presuming that the prepared particles are spheres, the average particle sizes of Samples A–G were calculated from the specific surface area data. Particles with an average size as small as ≈16 nm (Sample A) were synthesized. The maximum average particle size calculated was to be ≈105 nm (Samples D–F). Mixed powder prepared from fuel-rich reaction gel had a calculated average particle size ≈40 nm (Sample G). The average particle sizes estimated using BET measurement results and SEM photographs slightly differ, suggesting that spheres in SEM photographs are probably aggregates of finer particles, which cannot be resolved by the SEM.

As the combustion proceeds, fuel and oxidizing reagent are consumed. The consumption of the reagents is more complete if the initial fuel to oxidant molar ratio is close to the theoretical stoichiometric value. In oxidant- of fuel-rich precursors the excess of fuel or oxidant do not participate in the combustion reaction. However, due to the relatively high reaction temperature they are burned generating gases that loosen the just formed powder structure. On heating the nitrates decompose giving oxides and nitrogen [16]. Excess citric acid may also decompose producing gases (under reducing conditions may leave some carbon) or may react with oxygen from the air (especially, at the circumference of the pellet). The presence of the unreacted fuel or oxidant was followed by TG measurement of as-synthesized powders (Fig. 8). During heating in the air atmosphere up to 450 °C, Samples A–F did not show any significant mass changes while Sample G underwent several steps of mass loss (total mass loss up to 450 °C is 3.9%). This mass loss in Sample G indicates that a portion of initially present precursors did not react completely. Since during mass loss heating occurs only in the most fuel-rich sample possible, the initial oxidant excess decomposes entirely during the reaction while larger excess of fuel leaves some unreacted precursors.

All samples show a slight mass gain when heated above 500 °C (0.5–2.3%). From the color of the as-prepared powders it may be inferred that powders contain some

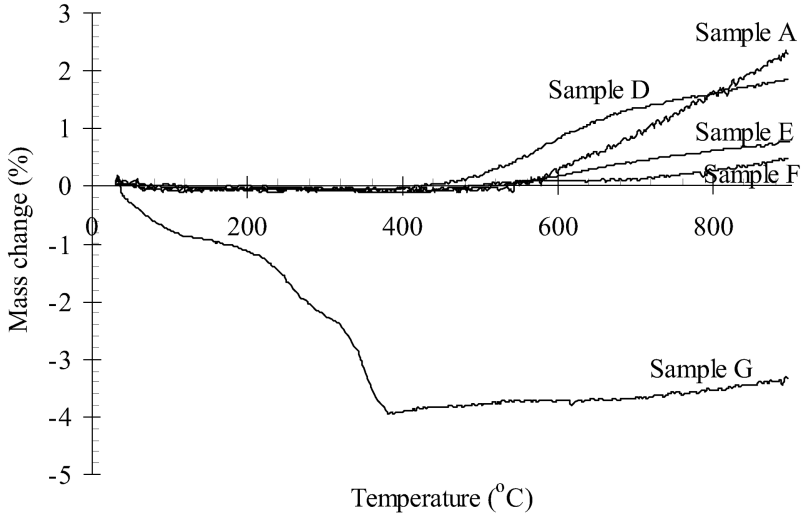

Fig. 8. TG plots of as-synthesized mixed powders in air.

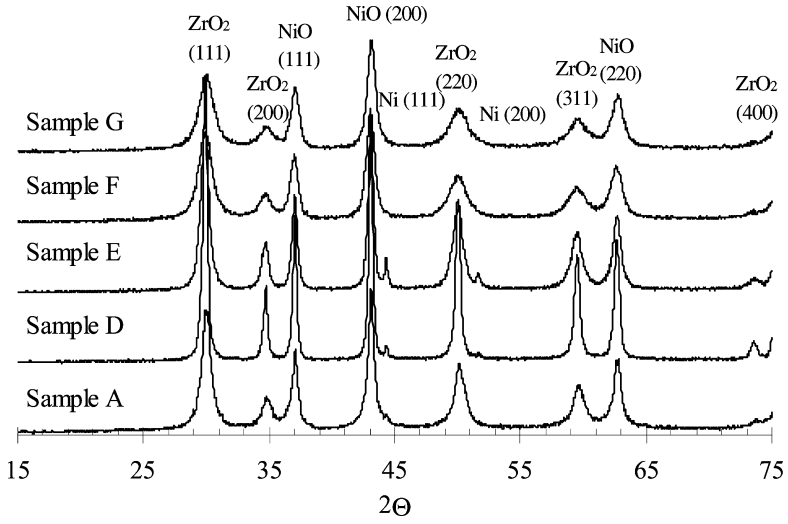

Fig. 9. X-ray diffraction spectra of the samples after synthesis.

metallic nickel as a product of precursor combustion (as later confirmed by the X-ray analysis). Furthermore, because of reductive atmosphere during synthesis, some non-stoiciometric oxides can be produced again changing the color from green to gray or black.

The phase content of the as-reacted powder also depends strongly on fuel amount in the precursor mixture. X-ray diffraction spectra of the product mixed powders, made from precursor mixtures with different fuel contents, are shown in Fig. 9. In all cases two main phases can be found corresponding to YSZ and NiO. One additional phase, determined as Ni phase, was found to be present in Samples D–F. According to the results obtained by X-ray analysis, only reaction mixtures D–F are rapid enough to hinder Ni particles from being oxidized completely to NiO. Another reason that prevents Ni particles to oxidize, are the localized reducing conditions resulting from the fuel combustion during the synthesis. On the other hand, owing to slow reaction rate, if the initial c/n ratio is oxidant- or fuel-rich, Ni phase does not appear in the as-reacted sample. Even though, the Sample G contained more reducing agent the slow combustion velocity nevertheless contributed to Ni oxidation.

The degree of crystallization is a function of the reaction temperature and time in which the material is exposed to high temperatures. Higher background and broader peaks obtained in the case of Samples A and G indicate a poorly crystallized powder mixture. Although these two samples react relatively slow (Sample A has to be heated all the time), the precursors with c/n initial ratio closer to the stoichiometric value reach higher reaction temperatures.

When heated up to 1000 °C in the air atmosphere the background in X-ray diffraction patterns in all samples diminishes and the peaks become sharper and more intense (Fig. 10). The peaks indicating Ni phase disappear due to NiO formation. However, diffraction peaks corresponding to

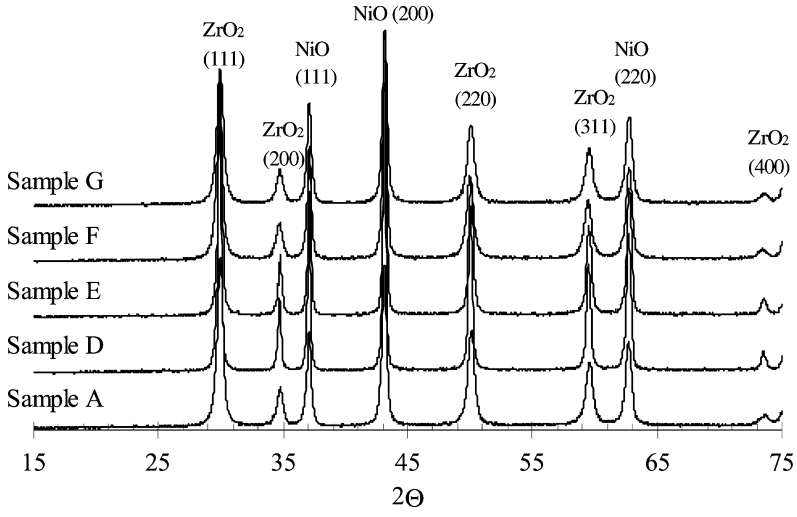

Fig. 10. X-ray diffraction spectra of the product mixed powders heated up to 1000 °C.

Samples D and E are much narrower when compared to those corresponding to Samples A, F and G. Broad peaks corroborate that grain sizes are considerably smaller when mixed powder is prepared from fuel or oxidant-rich initial gels. Smaller grain size after heating is a consequence of smaller grain size after the synthesis. From X-ray broadening of the peaks, average crystallite sizes in as-synthesized samples were calculated and found to be 7, 7, 17, 31 and 8 nm (plane YSZ (1 1 1)) and 16, 13, 23, 61 and 11 nm (plane NiO (1 1 1)) for Samples A, D, E, F and G, respectively. These values are in a relatively good agreement with the calculated grain size values from the specific surface measurements. During heating grains tend to grow. Calculated average crystallite sizes show that after heating up to 1000 °C grains are approximately twice as big as they were before thermal treatment (14, 15, 27, 37 and 15 nm plane YSZ (1 1 1); 24, 30, 65, 109 and 25 nm plane NiO (1 1 1) for Samples A, D, E, F and G, respectively).

After the synthesis the samples were milled and further thermally treated. The shrinkage curves of Samples A–G are depicted in Fig. 11. During sintering three different domains may be identified. In the range from 20 to 900 °C the samples exhibit normal volume expansion. At temperatures beyond 1100 °C fast shrinkage is observed, whereas at the end of sintering, the densification rate of the samples decreases drastically. The increase in the sintering rate at temperatures beyond 1100 °C is once more a function of fuel content in the initial reaction mixture. The samples prepared from reaction mixtures with lower c/n initial molar ratio (less fuel in the reactive gel; Samples A–C) start to sinter at slightly lower temperatures than the samples with higher initial additions of fuel. Consequently, they reach higher relative linear shrinkage at the end of sintering (Table 2). These samples exhibit a region of most intense sintering between 1250 and 1350 °C, while Samples D–G sinter at the highest relative sintering rate between 1350 and 1450 °C. Again, the higher the initial c/n ratio, the higher the temperature interval of an increased relative sintering rate. The estimated specific values from the shrinkage curves (e.g. start temperature of sintering (T_{start}), sintering temperature (T_{sinter}) and end temperature of sintering (T_{end})) are summarized in Table 2.

A comparison of the relative shrinkage, which decreases with the c/n initial ratio, indicates that higher fuel addition in the starting precursor inhibits the contraction of the fired composite powders (Table 2). Relative sintered densities

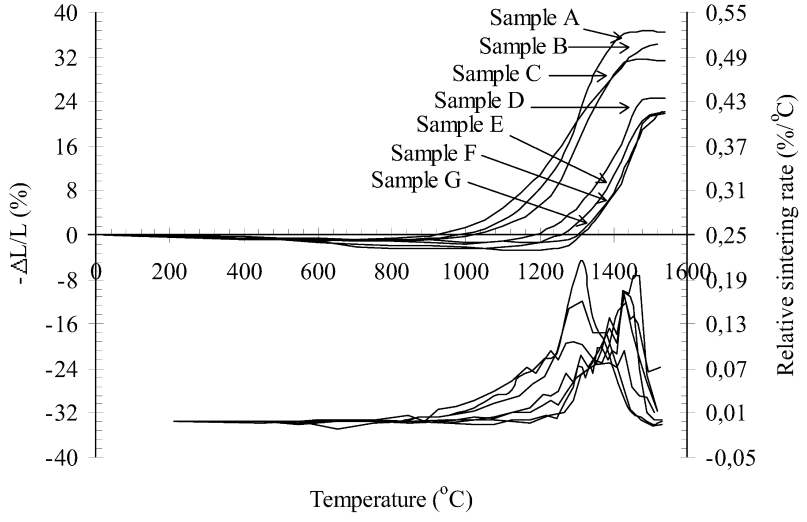

Fig. 11. Relative linear shrinkage and relative rate of sintering vs. temperature of Samples A–G.

Table 2
Sintering characteristics of Samples A–G

Sample	c/n[a]	Green density (g/cm^3)	Relative green density (%)	$-\Delta L/L$ (%)	T_{start} (°C)	T_{sinter} (°C)	T_{end} (°C)	Sintered density (g/cm^3)	Relative sintered density (%)
A	0.13	1.96	29.12	35.50	840	1320	1460	6.19	91.98
B	0.14	1.97	29.27	34.24	800	1300	1520	5.89	87.52
C	0.15	1.91	28.38	31.22	850	1300	1460	5.87	87.22
D	0.18	2.47	36.70	24.52	1000	1400	1500	5.85	86.92
E	0.23	2.79	41.46	22.14	1050	1420	1540	5.65	83.95
F	0.28	2.68	39.82	21.90	1200	1450	1540	5.60	83.21
G	0.33	2.66	39.52	22.20	1200	1420	1540	5.53	82.17

[a] Citrate/nitrate initial molar ratio.

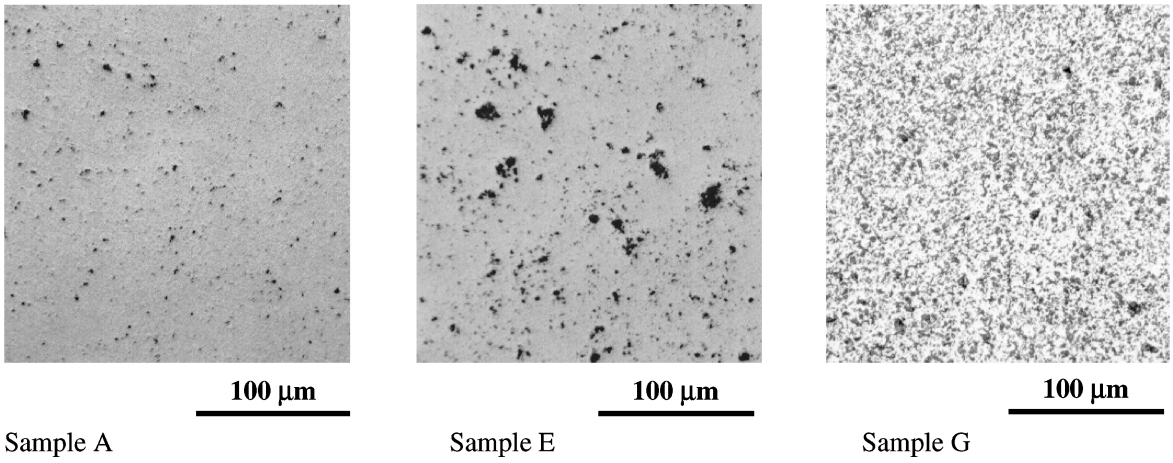

Fig. 12. Optical microscope images of the pellet microstructure of polished Samples A, E and G after sintering.

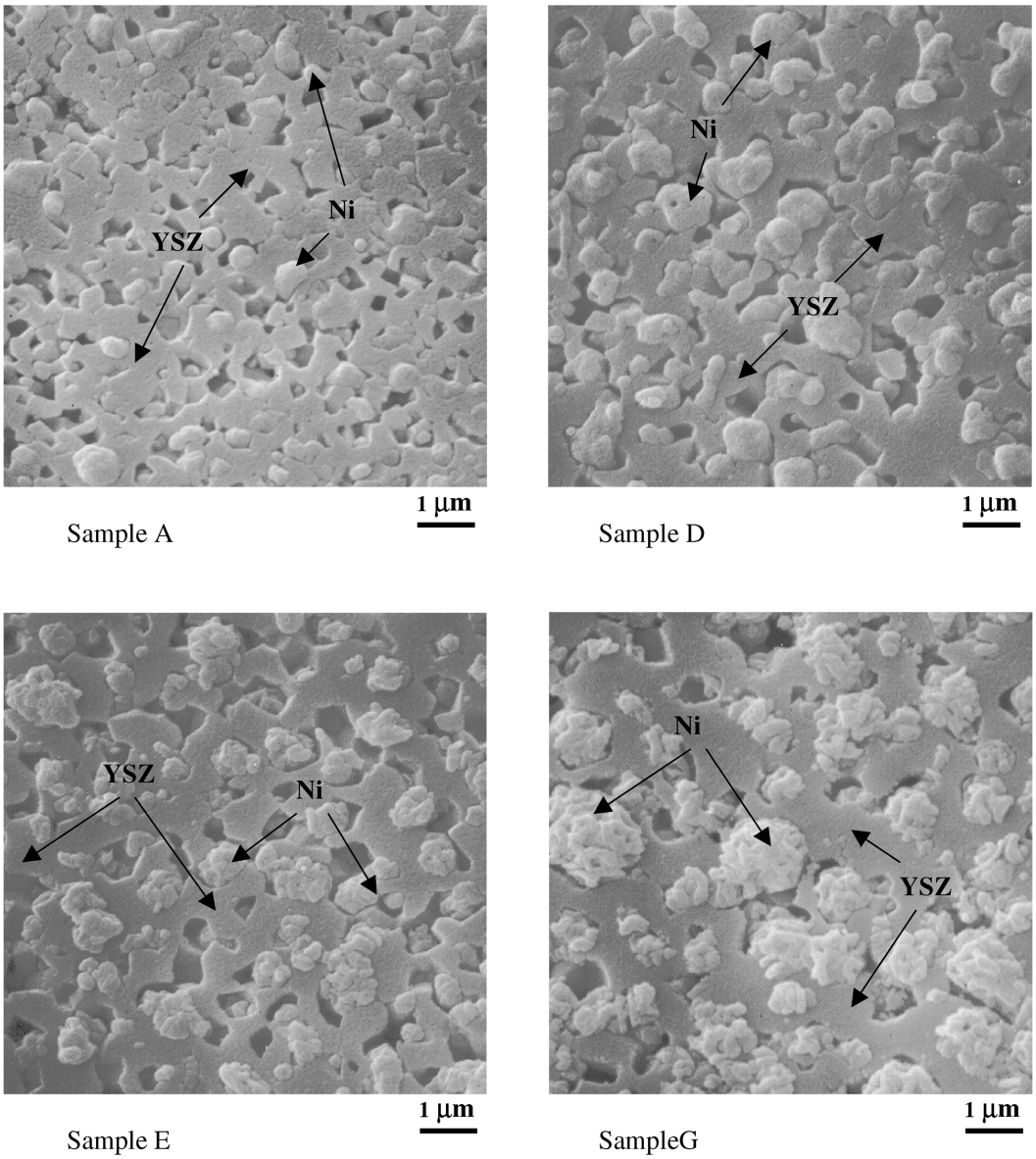

Fig. 13. SEM micrographs of polished and reduced samples A, D, E and G.

decrease with an increasing c/n initial ratio. Maximum sintered density, ≈92% of the theoretic density, as well as the relative shrinkage were reached in the case of Sample A (c/n = 0.13). Additionally, the high shrinkage of samples and their high relative densities (greater than 82% of theoretical value in all cases) result in a rather small degree of porosity in sintered samples.

Microstructures of sintered and polished Samples A, E and G as determined by optical microscopy are shown in Fig. 12. Sample A, at magnification 200× exhibits rather dense structure where no large pores are present. Heterogeneous pore size distribution is found to be present in sintered Sample E with areas of relative dense material structure and areas of highly porous structure. Porous structure is a characteristic pattern for Sample G too, however in this case the pore size distribution is much narrower as, for example, in Sample E.

During sintering a good contact between YSZ and NiO particles, respectively, has to be achieved. After firing, the YSZ particles must form a three-dimensional continuous network, rigid enough to withstand the contraction pressures, which occur during the reduction of NiO to Ni. In earlier work [15], it was shown that the continuity of YSZ rigid framework can be assumed, if there is no shrinkage of the composite during the reduction. Such rigid framework can be achieved if the amount of YSZ in the final composite exceeds 50%. This postulation was also partially the reason for the chosen nickel to zirconium source initial molar ratio. The continuity of both (ceramic YSZ and metallic Ni) phases must be preserved after the reduction as well.

Microstructure investigations of the reduced samples derived from the combustion synthesis are shown in Fig. 13. Micrographs of Samples A, D, E and G exhibit a good distribution of Ni particles inside YSZ matrix (Ni particles are represented by fine spherical grains captured inside the matrix). Fine Ni particles of the micro- or submicrometer range are distributed uniformly with fine pores surrounding them. There are no major differences in the composite microstructure among these samples. However, comparing the pore and the phase grain size distribution throughout the composite, it can be seen that Ni forms the smallest grains with the narrowest grain size distribution in the case of Sample A. These Ni grains are on submicrometer range while Ni grains in Sample G form a polydispersed system with grain sizes even larger than micrometer.

The Ni phase in all samples is randomly distributed inside the YSZ framework. From impedance measurements of Sample E, which show good electronic conductivity, we assume that the distribution of nickel is good enough to ensure continuity throughout the sample, thus, forming an uninterrupted electronic pathway (1.58 S/cm at 900 °C) (Fig. 14). Impedance spectra of other samples are very similar.

The plot of specific conductivity versus temperature for Sample E is shown in Fig. 15. Electrical conductivity of Sample E (likewise in all samples) decreases with increasing temperature, which is indicative of a metallic electronic conductor.

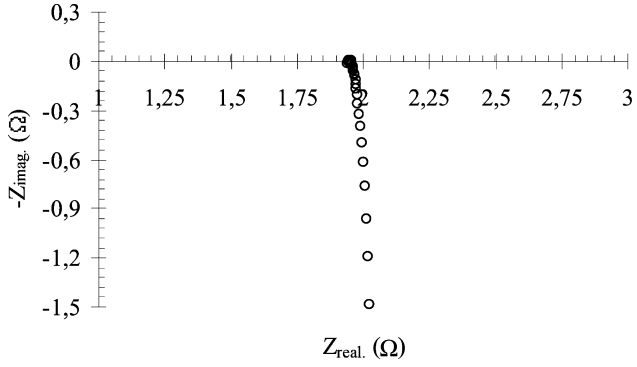

Fig. 14. Example of impedance spectroscopy data of Sample E produced via the combustion synthesis performed in 4 vol.% of H_2 and 96 vol.% of Ar atmosphere at 900 °C.

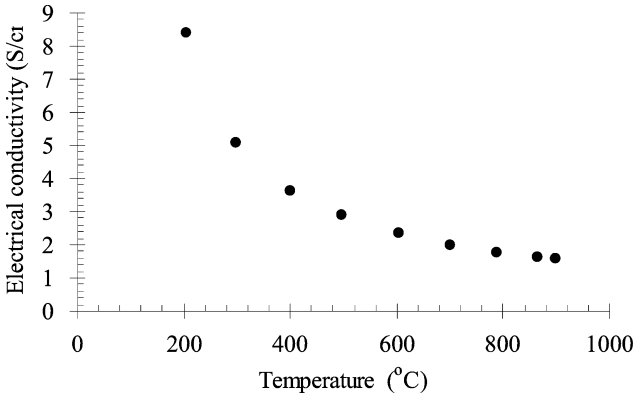

Fig. 15. Conductivity vs. temperature plot of Sample E.

4. Conclusions

Mixed oxide powders were prepared by the citrate/nitrate combustion synthesis that can produce final composite without employing any intermediate processes. Redox combustion reaction between metal nitrate and citric acid yielded ultrafine NiO–YSZ powders with average particle sizes on submicron level. The c/n initial molar ratio has a crucial influence on the combustion progressing and prepared powder characteristics. The combustion reaction is most vigorous with highest reaction temperatures if the c/n ratio prior to combustion is close to the stoichiometric value. Microstructure of the prepared final Ni–YSZ composite revealed that Ni particles are randomly distributed inside the ceramic framework. Good Ni distribution and appropriate Ni content (≈40 vol.%) ensured metallic conduction throughout the composite.

This investigation has shown that combustion synthesis process can be used to prepare composite materials suitable for SOFC anode manufacturing.

Acknowledgements

This work was supported by the Ministry of Education, Science and Sport, Republic of Slovenia.

References

[1] B. Riley, Solid oxide fuel cells—the next stage, J. Power Sources 29 (1990) 223–237.
[2] N.Q. Minh, Ceramic fuel cells, J. Am. Ceram. Soc. 76 (3) (1993) 563–588.
[3] N.Q. Minh, High temperature fuel cells. Part 2. The solid oxide cell, Chemtech 2 (1991) 120–126.
[4] E.C. Subbarao, H.S. Maiti, Solid electrolytes with oxygen ion conduction, Solid State Ionics 11 (1984) 317–338.
[5] J. Mizusaki, H. Tagawa, K. Naraya, T. Sasamoto, Nonstoichiometry and thermochemical stability of the perovskite-type $La_{1-x}Sr_xMnO_{3-d}$, Solid State Ionics 49 (1991) 111–118.
[6] S. Majumdar, T. Claar, B. Flandermeyer, Stress and fracture behavior of monolitic fuel cell tapes, J. Am. Ceram. Soc. 69 (1986) 628–633.
[7] N. Sakai, T. Kawada, H. Yokokawa, M. Dokia, T. Iwata, Sinterability and electrical conductivity of calcium-doped lanthanum chromites, J. Mater. Sci. 25 (1990) 4531–4534.
[8] T. Setoguchi, K. Okamoto, K. Eguchi, H. Arai, Effects of anode material and fuel on anodic reaction of solid oxide fuel cells, J. Electrochem. Soc. 139 (10) (1992) 2875–2880.
[9] C.H. Lee, C.-H. Lee, H.Y. Lee, S.M. Oh, Microstructure and anbodic properties of Ni/YSZ cermets in solid oxide fuel cells, Solid State Ionics 98 (1/2) (1997) 39–48.
[10] D.W. Dees, T.D. Claar, T.E. Easler, D.C. Fee, F.C. Mrazek, Conductivity of porous Ni–ZrO_2–Y_2O_3 cermets, J. Electrochem. Soc. 134 (1987) 2141–2146.
[11] S. Primdahl, M. Mogensen, Oxidation of hydrogen on Ni/yttria-stabilized zirconia cermet anodes, J. Electrochem. Soc. 144 (10) (1997) 3409–3419.
[12] J. Abel, A.A. Kornyshev, W. Lehnert, J. Electrochem. Soc. 144 (1997) 4253.
[13] T. Kawada, N. Sakai, H. Yokokawa, M. Dokiya, M. Mori, T. Iwata, Characteristics of slurry-coated nickel zirconia cermet anodes for solid oxide fuel cells, J. Electrochem. Soc. 137 (10) (1990) 3042–3047.
[14] T. Iwata, Characterization of Ni–YSZ anode degradation for substrate-type solid oxide fuel cells, J. Electrochem. Soc. 143 (5) (1996) 1521–1525.
[15] M. Marinsek, K. Zupan, M. Macek, Preparation of Ni–YSZ composite materials for solid oxide fuel cells anodes by gel-precipitation method, J. Power Sources 86 (1/2) (2000) 383–389.
[16] K.R. Venkatachari, D. Huang, S.P. Ostrander, W.A. Schulze, G.C. Stangle, A combustion synthesis process for synthesizing nanocrystalline zirconia powders, J. Mater. Res. 10 (3) (1995) 748–755.
[17] K.R. Venkatachari, D. Huang, S.P. Ostrander, W.A. Schulze, G.C. Stangle, Preparation of nanocrystalline yttria-stabilized zirconia, J. Mater. Res. 10 (3) (1995) 756–761.
[18] Z.A. Munir, U. Anselmi-Tamburini, Self-propagating exothermic reactions: the synthesis of high-temperature materials y combustion, Mater. Sci. Reports 3 (7/8) (1989) 277–365.
[19] A. Ringuede, J.R. Frade, J.A. Labrincha, Combustion synthesis of zirconia-based cermet powders, Ionics 6 (2000) 273–278.
[20] S.T. Aruna, M. Muthuraman, K.C. Patil, Synthesis and properties of Ni–YSZ cermet: anode material for solid oxide fuel cells, Solid State Ionics 111 (1998) 45–51.
[21] S.J. Kim, C.H. Jung, Y.S. Kim, Synthesis of ultrafine NiO–YSZ powders by GNP (glycine nitrate process), in: B. Thorstensen (Ed.), Proceedings of the 2nd European Solid Oxide Fuel Cell Forum, Oslo, Vol. 1, Druckerei J. Kinzel, Gottingen, 1996, pp. 321–330.
[22] U. Anselmi-Tamburini, G. Chiodelli, M. Arimondi, F. Maglia, G. Spinolo, Z.A. Munir, Electrical properties of Ni/YSZ cermets obtained through combustion synthesis, Solid State Ionics 110 (1/2) (1998) 35–43.
[23] S.R. Jain, K.C. Adiga, V.R. Pai Verneker, A New approach to thermochemical calculations of condensed fuel–oxidizer mixtures, Combust. Flame 40 (1981) 71–79.
[24] T. Hattori, S. Nishiyama, Y. Kishi, Y. Iwadate, Characterization of perovskite-type $GdFeO_3$ powders prepared by amorphous citrate process, J. Mater. Lett. 12 (1993) 883–885.
[25] D.J. Anderton, F.R. Sale, production of conducting oxide powders by amorphous citrate process, Powder Metalurg. 1 (1979) 14–21.